Available online at www.sciencedirect.com
SCIENCE DIRECT®
Journal of Power Sources 137 (2004) 117–127
JOURNAL OF POWER SOURCES
www.elsevier.com/locate/jpowsour

Role of the cathode and anode in heat generation of Li-ion cells as a function of state of charge

Hossein Maleki*, Jason N. Howard

Motorola Energy Systems Group (ESG), 1700 Belle Meade Court, Lawrenceville, GA 30043-6913, USA

Received 6 April 2004; accepted 1 May 2004
Available online 19 August 2004

Abstract

Thermal stability of Li-ion cells (from two different manufacturers, A and B) and their cathodes and anodes were evaluated as a function of state of charge (SOC) using accelerating rate calorimetry (ARC). Cell A was rated at 750 mAh and consisted of Sn-doped $LiCoO_2$ cathode and meso-carbon micro-fiber (MCMF) anode. Cell B was rated at 790 mAh and was comprised of a cathode and an anode made of $LiCoO_2$ and graphite. The electrolytes in cells A and B were mixtures of EC:EMC + 1M$LiPF_6$ and EC:EMC:DMC + 1M$LiPF_6$, respectively. ARC results indicated that between 50 and 125% SOC, the total heat generated by cell A is mostly dominated by self-heating of the cathode, while between 125 and 200% SOC the total heat generated by the cell was dominated by the anode. The total heat generated in cell B, however, was dominated by self-heating of the graphite anode, over the entire 50–200% SOC range. Also, the self-heating in cell B was higher than that for cell A. Heat generation of the $LiCoO_2$ increases with increasing SOC, and the Sn-$LiCoO_2$ heat generation reaches a maximum near 125% SOC. At low SOC, the temperature of the onset of chemical reaction (T_{OSCR}) for cell A was higher than that for the cell B. For both cells, at higher SOC, T_{OSCR} decreased with a sharp drop between 100 and 150% SOC. Overall results show that cell A offers a higher thermal stability than cell B. Also, the ARC test is more suitable than differential scanning calorimetry for correlation of cathode and anode heat generations to the thermal performance of full Li-ion cells.

Keywords: Thermal stability; Safety; Lithium-ion battery; Cathode and anode materials; Accelerating rate calorimetry; State of charge

1. Introduction

Rechargeable Li-ion cells have become the power source of choice for most portable electronic products (e.g., cell-phones and laptop computers) because of their high energy density, long cycle-life and high operating voltage range (2.8–4.2 V). A Li-ion cell typically consists of a carbon-based anode; a porous polymer membrane separator (polypropylene (PP) and/or polyethylene (PE)); and a lithium transition metal oxide cathode ($LiMO_2$, M = Co, Ni, and/or Mn). Mixtures of lithium salts and organic solvents provide an electrolyte medium for lithium ions to shuttle between the cathode and anode. During charge, lithium ions deintercalate from the cathode and intercalate into the anode, and the reverse process occurs during discharge. Passivating solid electrolyte interface (SEI) layers form predominantly on the anode during charge [1,2].

The nature of the SEI-layer on various carbons has been studied extensively [3–9]. The most comprehensive model suggests that the SEI-layer on the anode is composed of stable LiF, Li_2O and metastable Li_2CO_3 [6–8]. X-ray photoelectron spectroscopy results from Kanamura et al. [9] indicate that the SEI-layer of carbon anodes consist of Li_2O, LiOH, Li_2CO_3, $LiCO_2$-R and LiF when $LiPF_6$ is used as the salt. This SEI-layer breaks down at temperatures between 100 and 115 °C. Differential scanning calorimetry (DSC) and thermogravimetric analysis (TGA) studies have shown that the thermal breakdown of the SEI-layer on a carbon anode generates a small exothermic peak, accompanied by a corresponding loss of mass [10–12]. Thermal decomposition of cathode materials ($LiCoO_2$, $LiNiO_2$ and $LiMn_2O_4$) and their reactions with electrolyte have also been investigated using DSC, TGA and mass spectrometry [13,14].

The existing literature on thermal stability of Li-ion cell components—MCMB or MCMF anode and Li_xCoO_2 cathode in combination with organic electrolytes [EC: (DMC or MEC) + 1 M $LiPF_6$]—suggests the following sequence of thermal events occur when fully charged Li-ion cells are

* Corresponding author. Tel.: +1-770-338-3146; fax: +1-770-338-3144.
E-mail address: hosseinmaleki@motorola.com (H. Maleki).

0378-7753/$ – see front matter © 2004 Elsevier B.V. All rights reserved.
doi:10.1016/j.jpowsour.2004.05.053

heated [11,12]. First, the SEI-layer on the anode breaks down near 100 °C. Further chemical reactions then occur between the SEI-free anode and the electrolyte up to ~150 °C, leading to the formation of a fresh SEI-layer on the anode. Second, thermal decomposition of the cathode and reaction of that with electrolyte occurs between 150 and 165 °C and continues to near 235 °C. Finally, the Li_xC_6 reacts with the PVDF binder at temperatures near 250 °C [15]. These reactions are quite complex and highly dependent on the specifics of materials used and state of charge in the cell. Under normal charge conditions, the sequence of these thermal events should remain the same for cells using standard $LiCoO_2$ cathode, anode made of a carbon that is heat treated between 2200 and 2700 °C, and common types of electrolytes [e.g. EC: (DEC, DMC and/or EMC) + 1 M $LiPF_6$] and binders (e.g. PVDF and/or PTEF).

However, the main differences in the thermal stability of commercially available Li-ion cells can be related to materials selection and cell design, including: incorporation of heat retardant additives; thicker and higher melting point separator; the thickest possible cell-can and current collectors; ratios of electrodes coated versus uncoated areas over the current collectors; application of smoother and more rounded carbon particles; and $LiCoO_2$ stabilized by doping with transitional metals. The type of cathode material plays a critical role in the thermal runaway of Li-ion cells. D. Wainwright showed that a lower heat content is needed to force fully charged $LiNiO_2$ based cells into thermal runaway, compared to that needed for a fully charged cell using $LiCoO_2$ cathode [16]. The same studies also showed that the thermal runaway event in the $LiNiO_2$ Li-ion cells were more dramatic than that in $LiCoO_2$ cells. Therefore, many research groups (e.g. ANL, BNL, JPL, LBL and INEEL) are working on development of new cathode materials, particularly for EV/HEV applications.

During overcharge conditions complications arise from: interdependencies among the reactions, generation of by-products, and the presence of safety mechanisms such as thermal reaction control additives, meltdown separators, current interruption devices, and venting mechanisms.

Despite these complications, application of DSC/TGA in thermal stability studies of individual components and the correlation of these results with the thermal response of a full cell-can be useful in understanding and developing new/modified Li-ion cell materials with improved thermal properties. However, DSC provides limited insight into the true chemical stability of materials, which is important for designing safe Li-ion cells, because of its inability to accommodate large sample sizes. DSC results are also very sensitive to the sample preparation process. In DSC/TGA experiments, the sample-holder size, sample shape, particle size, quantity, packing inside of a sample-holder, and heating rate will all affect the results [17].

This work studies the thermal stability of two different prismatic Li-ion cells (rated at 750 and 790 mAh) and their components (full lengths of anode and cathode) at different states-of-charge (SOC) using accelerating rate calorimetry (ARC). Since ARC can use a larger sample size, we believe the technique provides more realistic data than DSC for understanding and correlating the thermal stability of the cathode and anode in Li-ion cells. ARC is becoming a more popular method among groups (e.g., battery groups at Sandia, Argonne and Lawrence Berkeley National Labs) investigating Li-ion batteries for EV applications.

2. Experimental

2.1. Sample preparation

Cells from manufacturers A and B were cycled five times between 3.0 and 4.2 V. Cells were charged/discharged at constant current (C/5). Charge steps were terminated once the current value tapered to 20 mA at a constant voltage of 4.2 V. After five cycles, the subsequent charge step was terminated when cells reached 50, 100, 125, 150 or 200% of their 1 C discharge capacity. Fig. 1A and B show voltage vs. capacity profiles of cells from manufacturers A and B, respectively, charged between 50 and 200%. Table 1 gives voltage and charge capacity values of the cells.

Thermal stability experiments of full cells or their electrodes were performed immediately after the final charging step. Cathode or anode was recovered from a charged cell and then transferred into a steel can similar to those used for 18,650 Li-ion cells. The can was then sealed using standard cell assembly techniques. All electrode preparation steps were carried out in a He-filled glove box. Table 2 includes information on the electrode material composition and physical parameters, as determined using cell construction analysis and scanning electron microscopy (SEM). General information on the composition of the electrolytes was provided by the cells' manufacturers; however, the exact compositions are proprietary. The electrolyte for cell A was 1 M $LiPF_6$ in a mixture of ethylene carbonate (EC) and ethyl methyl carbonate (EMC). The electrolyte for cell B was a 1M $LiPF_6$ in a mixture of ethylene carbonate (EC), ethyl methyl carbonate (EMC) and dimethyl carbonate (DMC).

X-ray diffraction (XRD) analysis showed a much higher degree of graphitization for MCMF than the graphite. The

Table 1
Charge and voltage values for prismatic Li-ion cells (rated at 750 and 790 mAh) for two different manufacturers, as a function of state of charge (SOC)

SOC (%) (mAh)	Cell A		Cell B	
	Capacity (mAh)	Voltage (V)	Capacity (mAh)	Voltage (V)
50	373	3.85 ± 0.030	395	3.93 ± 0.02
100	745	4.20 ± 0.014	790	4.21 ± 0.02
125	932	4.51 ± 0.015	–	–
150	1118	4.61 ± 0.017	1185	4.65 ± 0.03
200	1490	5.01 ± 0.020	1580	5.08 ± 0.03

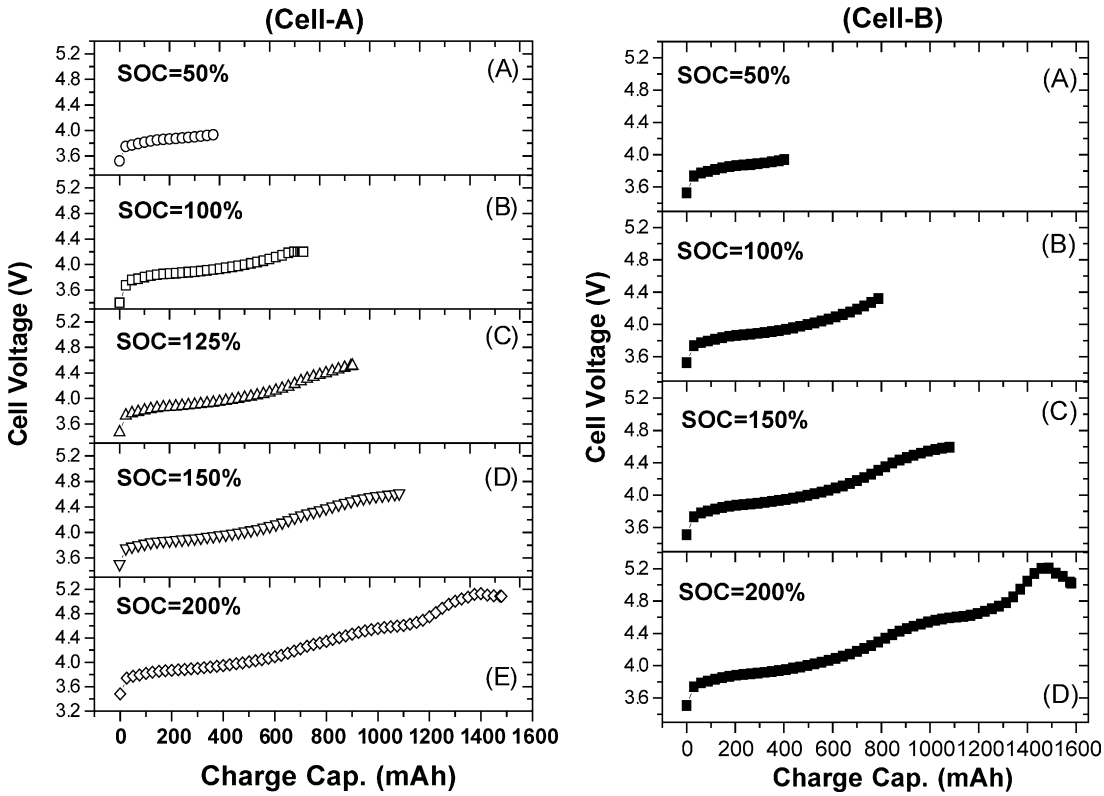

Fig. 1. Charge voltage vs. capacity profiles of cells from manufacturer-A (cell A) and manufacturer-B (cell B).

peak intensity counts for the (0 0 2)-plane of the MCMF and graphite were 11,000 and 6000, respectively. Similarly, there were noticeable differences in the crystal structure of the Sn-$LiCoO_2$ versus the $LiCoO_2$ electrodes. The (0 0 3)/(1 0 4) peak intensity ratios for the doped versus un-doped cobaltite samples were 30:1. For this analysis, cathode and anode samples were recovered from as received cells (OCV = 3.7–3.8 V) discharged to 2.5 V at C/20. Samples' binders were extracted by boiling them in methyl-ethyl-ketone (MEK) for 7–8 h and filtering at 70–80 °C. The process was repeated five times.

Fig. 2A and B are SEM photomicrographs of the cathode and anode from cell A. Fig. 3A and B show SEM photomicrographs for the cathode and anode from cell B. Fig. 4 shows DSC profiles of separators from cells A and B. Based on the melting temperature profiles, it is clear that cell A had a polyethylene (PE) separator; and cell B a polypropylene/polyethylene/polypropylene (PE/PP/PE) tri-layer

Table 2
Components characteristics of the prismatic Li-ion cells (A and B) from two different cell manufacture: data obtained using cell construction, SEM, EDX and light microscopy

Product	Parameters	Anode	Separator	Cathode
Cell A	Material	MCMF	Single layer (PE)	Sn-$LiCoO_2$
	Size (μm)	Particles 35–100	Thickness 22	Particles ≤ 10
	Active area (cm^2)	257.88	432.6	242.53
	Thickness (cm)	0.016	0.0020	0.018
	Density (g/cm^3)	1.4	N/A	2.8
	Binder type	PTEF	N/A	PVDF
	Binder content	(7–8 wt.%)		(3.5–4 wt.%)
Cell B	Material	Graphite	Tri-layer (PP/PE/PP)	$LiCoO_2$
	Size (μm)	Particles 10–25	Thickness 25	Particles 20–55
	Active area (cm^2)	340.56	374	324.24
	Thickness (cm)	0.014	0.0025	0.012
	Density (g/cm^3)	1.3	N/A	3.2
	Binder type	PTEF	N/A	PVDF
	Binder content	7–8 wt.%		4–5 wt.%

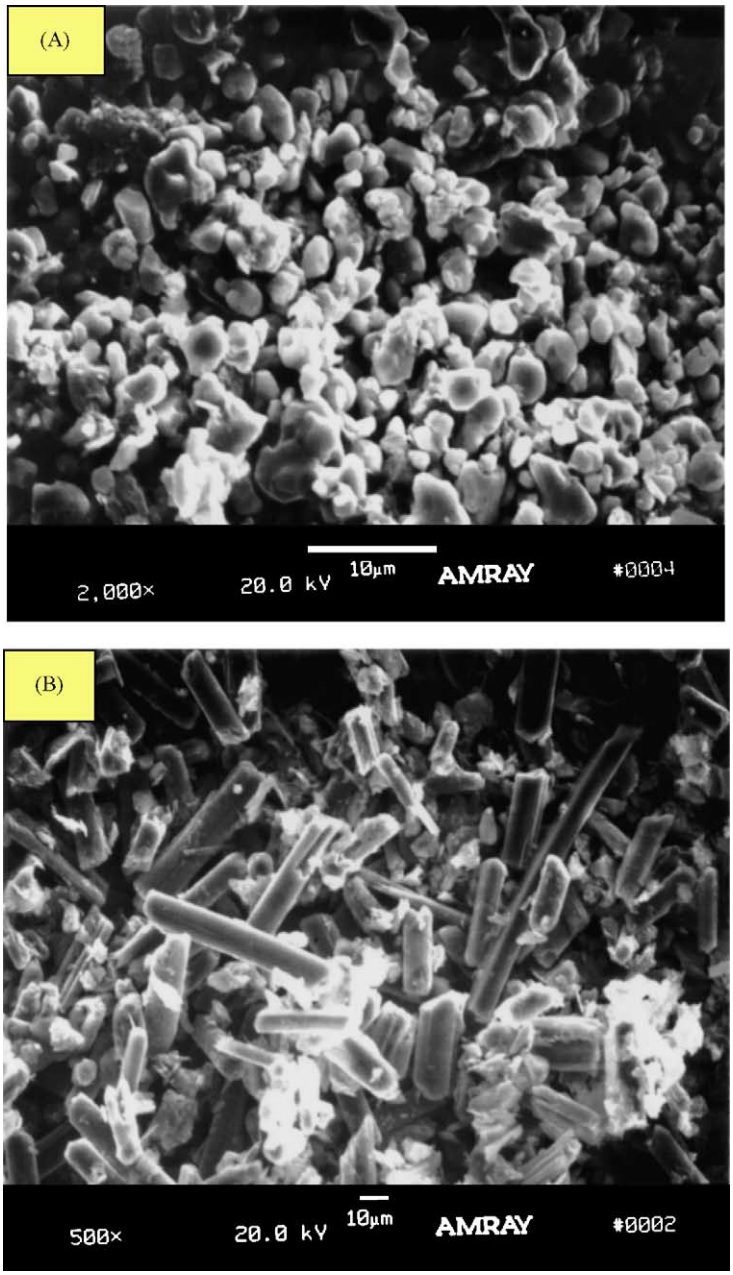

Fig. 2. SEM micrograph of cathode (A) and anode (B) from cell A.

separator. The tri-layer separator provides a wider temperature window (130–160 °C) than single-layer PE (130–145 °C) for thermal shutdown.

2.2. Thermal stability studies

Accelerating rate calorimetry (ARC) measurements were performed on a Columbia Scientifics Instrument. ARC measurements in the heat-wait-search (HWS) mode were used to determine the thermal response (temperature versus time) and self-heat-rates (SHR, °C/min) of full cells and their anodes or cathodes. A lightweight aluminum fixture was used to suspend the sample and sample-holder assembly (SSHA) in the center of the ARC heater cavity. The SSHA was heated from room temperature to 405 °C in 10 °C steps at 20 °C/min. At the end of each heating step, 40 min of wait-time was allowed for the ARC and SSHA to reach equilibrium. In HWS mode, the ARC searches for a SSHA temperature rise of 0.02 °C/min or higher at the end of each wait period. If this SHR is detected, the ARC switches to the adiabatic mode and tracks the exothermic activity of the sample. Otherwise, the ARC proceeds to the next heating step. Details and criteria for sample holder design and sample size are described elsewhere [12,18].

In these experiments, the ARC was unable to track the self-heating of cells closely during thermal runaway above

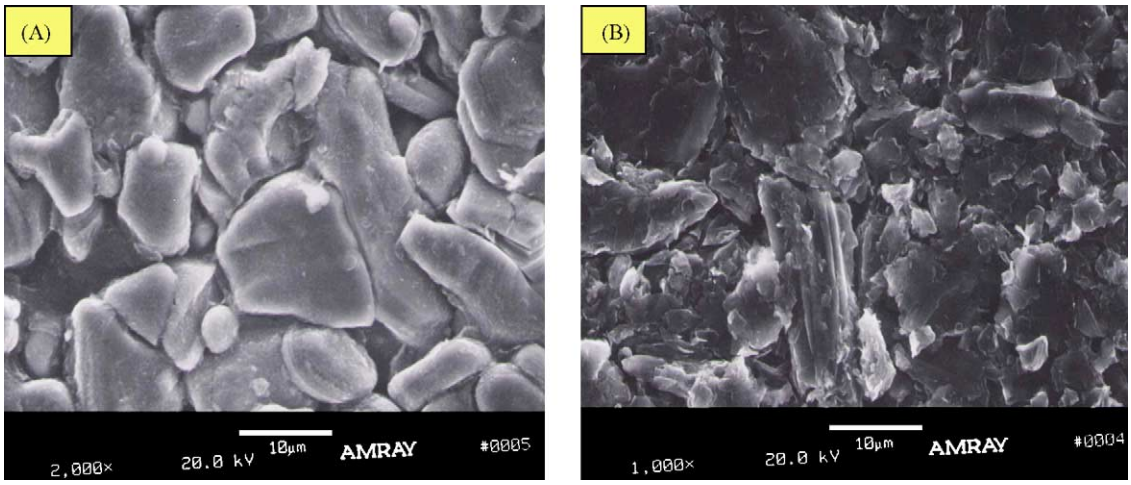

Fig. 3. SEM micrographs of cathode (A) and anode (B) from cell B.

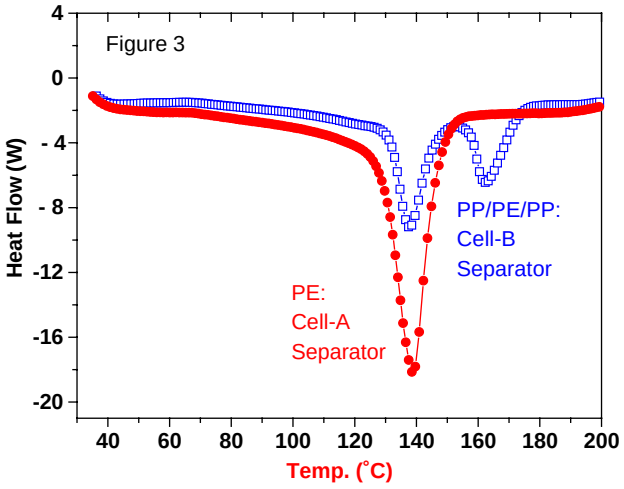

Fig. 4. Differential scanning calorimerty (DSC) profiles of the separators from cells A and B.

200 °C because the instrument is limited in its ability to supply sufficient heat to maintain a completely adiabatic condition. Therefore, we have focused on the temperature of onset of chemical reaction (T_{OSCR}) and heat generation values up to 200 °C. This information is generally sufficient for thermal analysis of Li-ion cells for portable electronics applications.

3. Results and discussion

3.1. Self-heating in cell A

Fig. 5A and B show the temperature versus time and SHR versus temperature profiles for cell A under various SOC. The T_{OSCR} decreases as the SOC increases from 50 to 200%. Except for the 50% charged cell, all others went to thermal runaway. "T_{OSCR}" is defined as the temperature when the

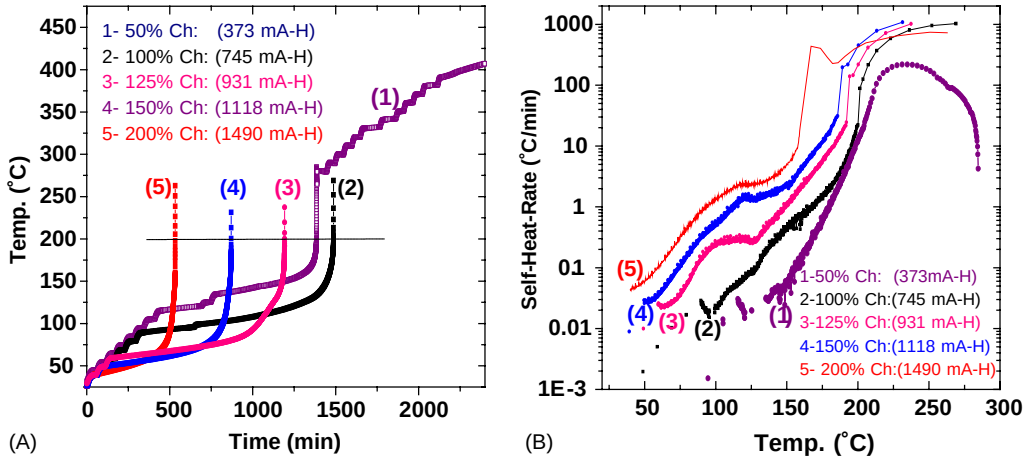

Fig. 5. Temperature vs. time and self-heat-rate vs. temperature profiles for cell A at 50–200% SOC. All cells went to thermal runaway except the one at 50% SOC.

sample SHR reaches the level of ARC minimum thermal detection limit (0.02 °C/min) and continues to grow. Under normal circumstances batteries are operated in non-adiabatic environments. In this case, T_{OSCR} depends on the heat generation and heat dissipation capability of the cell. Richard and Dahn [19] described a method of predicting the thermal behavior of a Li-ion cell using a combination of heat generation data from the ARC test and measuring heat dissipation data from the cell-can. This study shows that the onset of chemical reaction that could lead to thermal runaway, in a fully charged 18,650 Li-ion cell, should start at 140 °C, where the heat generation, primarily from the anode, exceeds the heat dissipation of the cell.

3.2. Cathode

Fig. 6A is a superposition of SHR versus temperature profiles of cathodes from cell A charged between 50 and 200%. The 50 and 100% charged samples self-heat continuously, starting near 150 and 130 °C, respectively. The heat generation is attributed to the start of thermal reaction of the electrolyte with evolved oxygen from the delithiated cathode, as well as cathode material decomposition. However, the continuity of the self-heating profiles indicates the availability of a sufficient quantity of electrolyte and oxygen to cause the reaction to continue and heat generation to increase. Dahn et al. [13] showed the occurrence of oxygen mass loss from $LiCoO_2$ as function of temperature using a combination of thermogravimetric analysis (TGA) and mass spectrometry (MS). This mass loss started near 150 °C and reached a maximum near 250 °C.

Discontinuity of the SHR of the 125% charged samples, as opposed to the 50 and 100% charged samples, between 50 and 112 °C is due to the presence of small exothermic reactions that keep falling below the sensitivity of the ARC limit (0.02 °C/min) in detecting the sample SHR. This also suggests the presence of thermally unstable materials on the surface of the cathode; or changes in electrolyte that lowers its thermal reactivity with oxygen between 50 and 112 °C. The main self-heating for this sample started near 112 °C and is attributed mainly to thermal reaction of electrolyte and the evolved oxygen from the cathode.

The SHR versus temperature profile of the 150 and 200% charged samples both have two main thermal reaction peaks, in addition to the presence of small exothermic reactions in the low temperature side. For the 150% charged sample, the first main SHR (S1) is between 78 and 166 °C with a maximum near 95 °C, and the second SHR (S2) starts at 150 °C. The 200% charged sample follows the same trend as the 150% charged sample, except that the onset of both main SHRs are shifted toward higher temperatures.

Unlike studies on the thermal stability of the SEI-layer on carbon-based anode materials, there is very little information on the existence of passivation layers on the surface of cathodes [20,21]. The studies report formation of SEI-layers of Li_xCoO_2 due to its reaction with electrolyte and extended cycling.

Our studies show the existence of two main mechanisms in the thermal decomposition of the delithiated cathode and its reaction with electrolyte. The exact nature of this two-step process in SHR of the 150 and 200% charged samples is not clear. However, it is known that the Li_xCoO_2 is highly unstable, especially when delithiated above its structural stability ($x < 0.5$) [13]. Therefore, it is possible that oxygen evolves due to self-heating of the cell during overcharge. Then, the evolved oxygen reacts with electrolyte and forms layers of passivating-products on the surface of the cathode. Thermal breakdown of these byproducts appear as small exothermic peaks for the 125% charged sample, between 50 and 112 °C, before the beginning of the first main self-heating step (S1). In the cases of the 150 and 200% charged samples, the cell temperature rises to higher values than that for the 125% sample during overcharge and at the same time quantities of the evolved oxygen is larger. Therefore, it is possible that

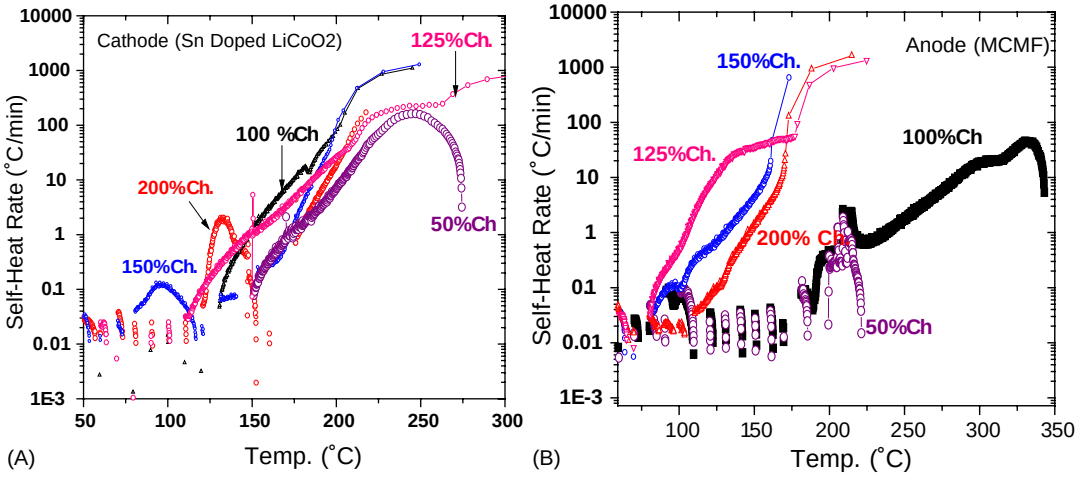

Fig. 6. Self-heat-rate vs. temperature profiles of the cathode (A) and anode (B) recovered from cell A at 50, 100, 125 150 and 200% SOC.

the combination of higher temperature and larger oxygen content leads to the formation of passivating products of different thermal stability. These could be the reason for the differences in thermal behavior of the 100% charged sample versus samples charged to higher values.

DSC studies have indicated that the thermal reaction of delithiated Li_xCoO_2 ($1 < x < 0.014$) with organic electrolytes generally occurs between 150 and 170 °C, with no major exothermic reactions at lower temperatures [12–14]. If this indeed is the case, then there is a difference between using the DSC or the ARC to determine the thermal stability of Li-ion cell materials. In principle, DSC is a more sensitive technique than ARC. However, its inability to accommodate large sample size limits its application to small sample sizes. Furthermore, DSC generally does not clearly show the presence of small heat generating reactions at lower temperature because of continued heating of the sample by a secondary source. ARC, on the other hand, can determine the thermal stability of electrodes matching those found in a real Li-ion cell. Therefore, the ARC test is more suitable than DSC for understanding the thermal behavior of cathode and anode, as well as their impact on the safety of a real Li-ion cell.

3.3. Anodes

Fig. 6B shows the superimposition of SHR profiles of the anodes from cell A charged between 50 and 200%. The SHR trends for the 50 and 100% charged samples are similar, except that the latter sample self-heats for a longer time. Both samples show a series of small exothermic peaks, up to around 170 °C, that is attributed to thermal breakdown of the SEI-layers on MCMF. This result agrees with prior DSC data obtained in our laboratory (results not published). The self-heating of the 125, 150 and 200% charged samples start at lower temperatures than that observed for the 100% charged sample. The major portion of the self-heating for the 125% charged sample occurs at lower temperature than the other samples.

The overall results suggest the total heat generation of the SEI-layer on the 50% charged sample is not high enough to initiate reaction of the Li_xC_6 with the anode binder material. No thermal runaway was observed for this sample. For the 100% charged sample, though, thermal reaction of LiC_6 with the binder starts near 210 °C and continues until the end of the experiment. For the samples charged from 125 to 200%, the thermal reactions between SEI-layer, $Li_{(1+x)}C_6$ and anode binder occur in a narrow temperature range with no time lag between them, unlike that in the 50 and 100% charged samples. The rates of exothermic reaction and heat generation among these overcharged samples are also higher than the sample charged to 100%. These are attributed to heat generation from thermal reactions of plated lithium and anode-electrolyte reaction byproducts formed during overcharging of the cell. From a practical standpoint, fast and continuous self-heating causes thermal runaway in a short time, since a Li-ion cell-can only accommodate a limited rate of heat generation by its thermal mass and heat dissipation.

3.4. Comparison of cathode, anode, and cell

Fig. 7A–D compare the SHR of cell A charged to 50, 100, 150 and 200% with the SHR for its cathode and anode also

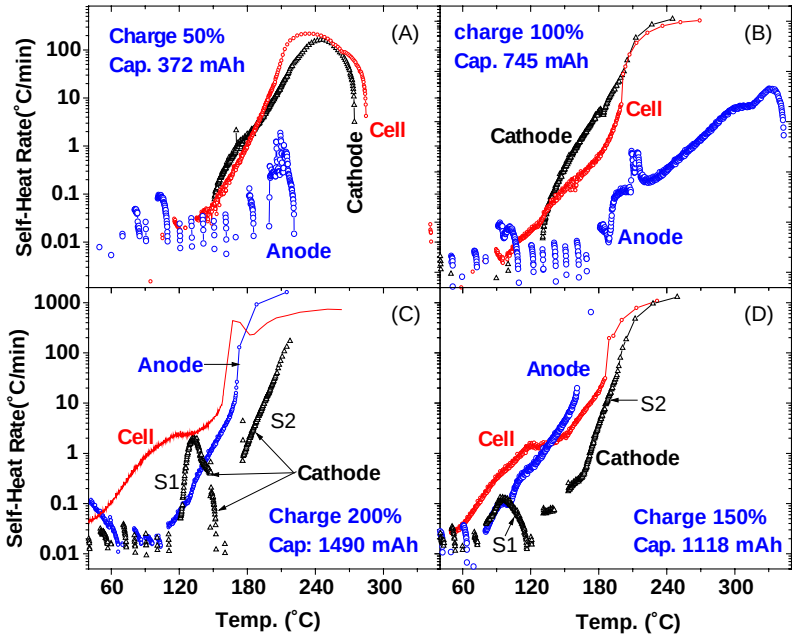

Fig. 7. Comparison of self-heat-rates (SHR) profiles of cell A and its cathode and anode at 50–200% SOC: SHR temperature range changes with increasing SOC.

charged to the corresponding SOC. For the 50 and 100% SOC (Figs. 7A and 6B), the cathode SHR is higher than the anode and also closer to the SHR for the full cell. These indicate the total heat generation in full cell A, at 50 and 100 % SOC, is dominated more by the self-heating of the cathode than the anode. The initial T_{OSCR} in cell A is primarily determined by the heat generation from the small exothermic reactions formed by thermal decomposition of the SEI-layer on the anode.

At 150% SOC (Fig. 7C), a major portion of the full cell SHR is aligned with the anode. This can be attributed to the presence of plated lithium and reaction byproducts formed from overcharging the cell. These increase the quantity and rate of reaction in the anode with increasing temperature. Here, the cathode first major SHR (S1) stays closer to the SHR of the full cell and the second SHR (S2) moves further toward the higher temperature side. However, contrary to the cases of 50 and 100% charged samples, it is clear that the anode plays a bigger role than the cathode in thermal runaway of cell A because its SHR is closer than that for cathode to SHR of full cell A. In addition, the onset of thermal reactions for the anode occurs at a lower temperature.

At 200% SOC (Fig. 7D), the cathode and anode both show the same trends of SHR as the 150% SOC, with respect to SHR of the full cell. The first major portion of cathode SHR (S1) moves toward a higher temperature and also grows at a faster rate and has a higher maximum. The difference between the S1 peaks in the 150 and 200% charged sample could be related to differences in the oxygen content of these samples and/or byproducts of their reactions with electrolyte. Both samples show a series of small exothermic reactions before starting their major portions of the SHRs. However, it appears that the accumulative heat of these small reactions from both cathode and anode is high enough to push the full cell into thermal runaway.

3.5. Self-heating cell B

Fig. 8A and B show the profiles of temperature versus time and SHR versus temperature for cell B under various SOC. The T_{OSCR} decreases as the SOC increases from 50 to 200%. Except for the 50% charged cell, all others went to thermal runaway. Cell B shows the same overall thermal behavior as cell A, except that the same reactions cause the main portion of self-heating of the cell at 200% SOC to occur at higher temperature than the cell at 150% SOC. This surprising result may be due to the fact that some of the early heat-generating reactions have occurred during the overcharging process itself. This would mean that less thermally active materials were available for heat production during the ARC test. One possible factor to support this hypothesis is that cell B had lower heat dissipation capability than cell A. Therefore, cell B may have reached a higher temperature during overcharge, especially that for the 200% SOC where high heat had consumed materials “pre-reactions” before the ARC test.

3.6. Comparison of cathode, anode, and cell

Fig. 9A–D compare SHR of cell B at 50, 100, 150 and 200% SOC versus the SHR of its cathode and anode also charged to the corresponding SOC. Self-heating of cell B and its electrodes are higher than that for the cell A, even though both cells show nearly similar trends. The higher heat generation in cell B versus cell A is attributed to the higher exothermic heat of the reaction from graphite than the MCMF with electrolyte. Such results were confirmed using DSC tests that showed the exothermic heat generation of fully lithiated graphite (1220 J/g) is nearly twice that of fully lithiated MCMF (648 J/g) [12].

For the 150% charged sample, however, the early portion of cell B SHR is dominated by the self-heating of the anode and the second portion more by cathode. The 200%

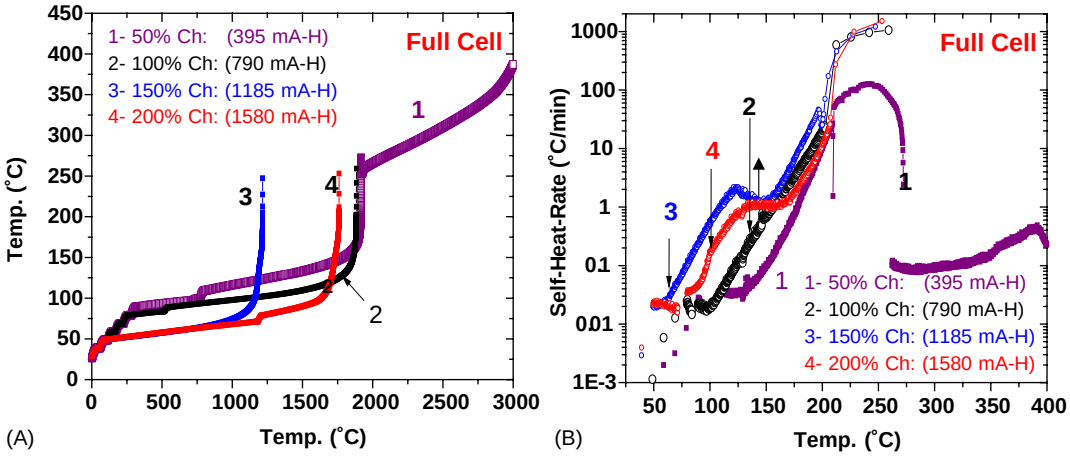

Fig. 8. Temperature vs. time and self-heat-rate vs. temperature profiles for the cell B at 50–200% state of charge: all cells went to thermal runaway except the one at 50% SOC.

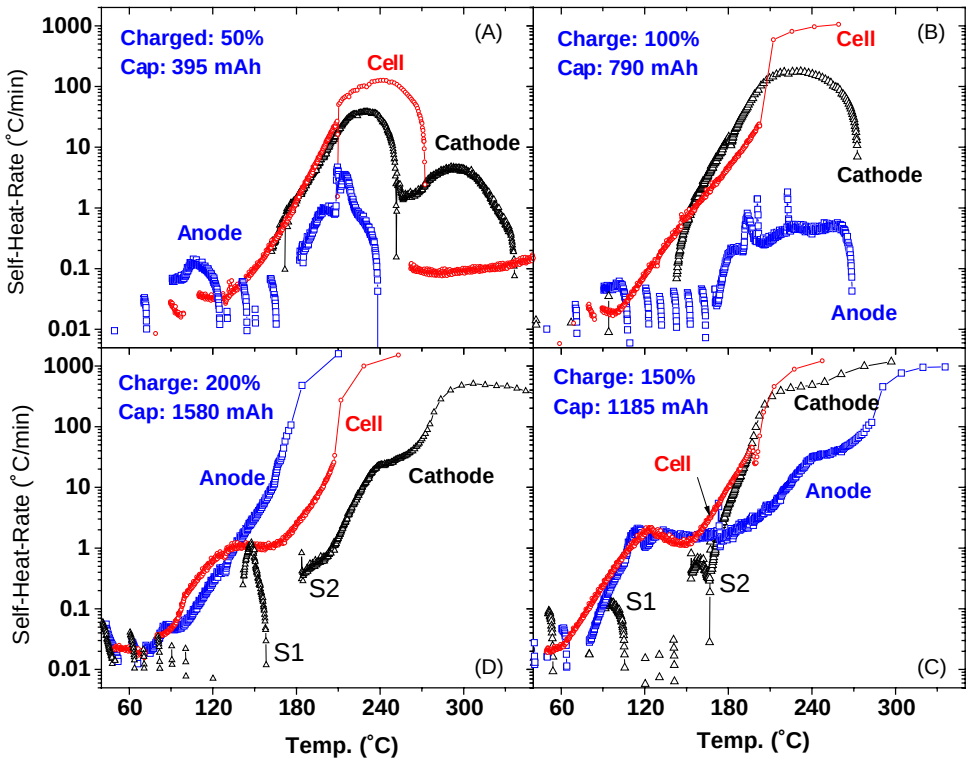

Fig. 9. Comparison of self-heat-rates (SHR) profiles of cell B and its cathode and anode at 50–200% SOC: SHR temperature range changes with increasing SOC.

SOC graphite anode starts self-heating "continuously" at a lower temperature (65 °C) than MCMF (110 °C), which has a series of small exothermic reactions at lower temperatures. This suggests that, in an overcharged cell, this graphite plays a more dominant role than MCMF in pushing the Li-ion cell into thermal runaway. The S1 peak in the cathode of the 200% charged cell starts at 125 °C and for the 150% charged cell starts near 75 °C. The 200% charged sample includes more numbers of smaller exothermic reactions than the 150% charged sample, which has fewer of the larger reactions. Heat generation analysis (J/g) using the ARC software showed the accumulative heat of these small reactions, up to 120 °C range, for the cathode of the 200% charged cell was less than 1/4 of that for the 150% charged sample. This may be attributed to partial destruction of thermally active materials because of cell self-heating during overcharge to 200%. In this case, some of the active materials in the cell passivate and therefore do not participate in self-heating of the cell during the ARC test. We believe these are the reasons that the 150% charged cell started thermal runaway at a lower temperature than the 200% cell.

3.7. Cells A and B T_{OSCR} and total heat generation

Fig. 10 shows the T_{OSCR} in cell A and B between SOC values of 50 and 200%. There is a sharp drop in the T_{OSCR} of cells at 100% versus 125% SOC. These results suggest the possibility that in cells charged between 125 and 150%, plated lithium and component reaction byproducts all are at their highest level of reactivity. However, charging the cell above 150% reduces thermal reactivity of the cathode, which leads to slowing down or leveling off the decrease in T_{OSCR} in a full cell. The exact nature of such differences in thermal stability of delithiated doped versus un-doped $LiCoO_2$ is not clear. However, it is well known that incorporation of dopants (transition metals, such as Al and Sn) improves the

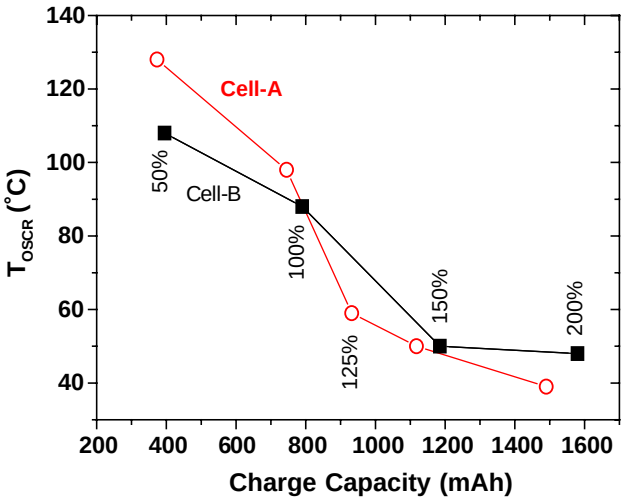

Fig. 10. Plots of the temperature onset of chemical reactions (T_{OSCR}) vs. charge capacity values (mAh) for the cells A and B at 50–200% SOC.

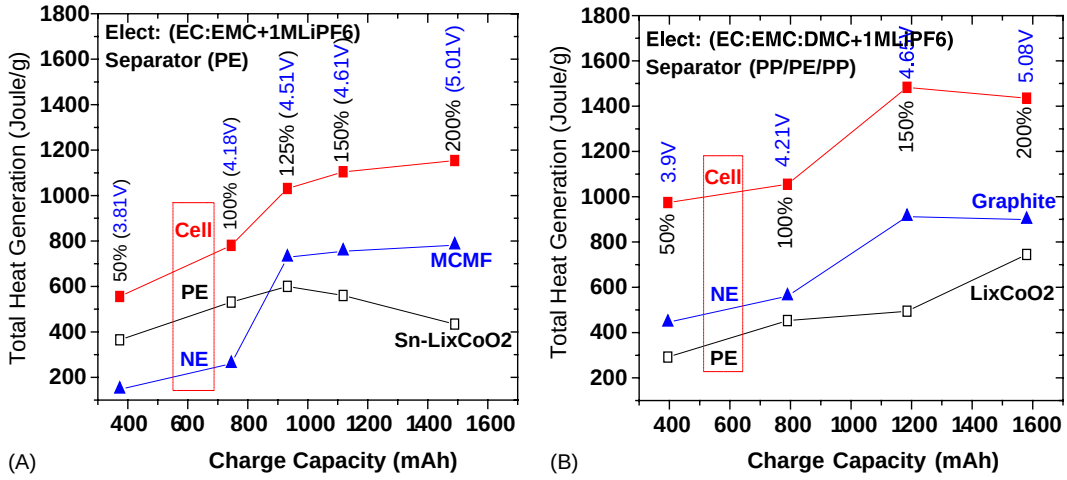

Fig. 11. Plots of heat generation values for the cells A and B and their cathodes and anodes at 50–200% SOC. Heat generation values were calculated from beginning of the self-heating up to 200 °C using the ARC software.

structural stability of lithium cobaltates that leads to a higher thermal stability. One observation worthy of noting is that, after cell autopsy, the components of 200% charged cells appeared dryer than cells partially overcharged.

Fig. 11A and B are plots of heat generation values (J/g) of cells A and B and their cathode and anodes, respectively. The overall results show that in cell A total heat generation is dominated by the total self-heating of the cathode up to near 125% SOC. From SOC values greater than 125%, the anode plays a more dominant role than the cathode. For cell B, however, the self-heating of the anode is more dominant than the cathode at all SOCs. The thermal response of a full cell is different than the sum of the anode and cathode.

There are several reasons for the noted variance in thermal behavior of cell A versus cell B. These may include: differences in the thermal mass, interdependencies in the reactions between the electrodes and electrolyte, geometrical differences, differences in the internal pressure, and finally the loading ratios of masses of active cathode to anode materials. Here, the mass loading ratios of active materials in cell A (2.21) were slightly higher than that in cell B (2.06). This difference, however, most likely had small effects on the differences in thermal behavior of these cells and their components as a function SOC versus temperature. The lower heat generation of MCMF versus graphite anode is mainly related to its lower surface area and smoother surface morphology. Studies by Dahn's group [20] notes surface area of about 0.4 m^2/g for pitch-based carbon fiber (BP Amoco) and 4.3 m^2/g for synthetic graphite SFG-44 (Timcal). Using ARC, they also showed that thermal stability of lithiated carbon fiber is noticeably higher than lithiated graphite.

4. Conclusion

Thermal stability of two prismatic Li-ion cells, charged between 50 and 200%, was evaluated using an accelerating rate calorimetry (ARC). Results indicated the cell consisting of Sn-$LiCoO_2$ cathode and meso-carbon micro-fiber (MCMF) anode offers a higher thermal stability than the cell consisting of $LiCoO_2$ cathode and graphite anode. This difference is attributed mostly to the higher thermal stability of MCMF over graphite. Heat generation of the $LiCoO_2$ increases as the SOC of the material increases from 50 to 200%. In contrast, heat generation in the Sn-$LiCoO_2$ cathode has a maximum at a SOC value near 125%. Total heat generation of these Li-ion cells increase more rapidly at SOC values between 100 and 150% than at SOC values below 100% or greater than 150%. Results also showed the presence of two distinct self-heating peaks for the cathodes from both cells charged to higher than 100%. Such phenomena may be attributed to the reactions of overcharged $LiCoO_2$ with electrolyte that lead to formation of layers of unstable, thermally active materials on the surface of the cathode. With increasing temperature, these layers tend to break down before the main reactions of the $Li_{(x<0.5)}CoO_2$ with electrolyte begin.

In conclusion, the results show that the thermal responses of both cathode and anode in a Li-ion cell are a dynamic process controlled by their SOC, interactions of self-heat-rates, and the total heat generated by each component. Furthermore, we observed differences in results obtained by using ARC versus DSC. The larger sample size available in ARC experiments is more likely to represent real world cell behavior.

Acknowledgements

The authors would like to thank Ganesh Venugopal (Motorola Energy Systems Group) for his contribution to this work.

References

[1] D. Aurbach, M.D. Levi, E. Levi, B. Markovsky, G. Salitra, H. Teller, in: C.F. Holmes, A.R. Landgrebe (Eds.), Batteries for Portable Applications and Electric Vehicles, PV 97 -18, The Electrochemical Society Proceeding Series, Pennington, NJ. 1997, p. 941.

[2] E. Peled, D. Golodintsky, G. Ardel, J. Electrochem. Soc. 144 (1997) L208.

[3] R. Fong, U. von Sacken, J.R. Dahn, J. Electrochem. Soc. 137 (1990) 2009.

[4] R. Yazami, in: G. Pistoia (Ed.), Lithium Batteries: New Materials, Developments and Prospective, Elsevier, New York, 1994, p. 49.

[5] D. Aurbach, Y. Ein-Eli, O. Chusid, Y. Carmeli, M. Bakai, H. Hamin, J. Electrochem. Soc. 141 (1994) 603.

[6] E. Peled, D. Golodnitsky, G. Ardel, J. Electrochem. Soc. 144 (1997) L208.

[7] D. Aurbach, Y. Ein-Eli, B.B. Markovsky, A. Zaban, S. Luski, H. Yamin, J. Electrochem. Soc. 142 (1995) 2882.

[8] K. Kanamura, H. Tamura, S. Shiraishi, Z-I. Takehara, J. Electroanal. Chem. 394 (1995) 49.

[9] K. Kanamura, H. Takezawa, S. Shiraishi, Z-I. Takehara, J. Electrochem. Soc. 137 (1990) 2009.

[10] C. Menachem, D. Golodnitsky, E. Peled, Electrochemical Society and International Society of Electrochemistry Proceeding, abstract no. 138, Paris, France, 1995, p. 157.

[11] A. Du Pasquier, F. Disma, T. Bowmer, A.S. Gozdaz, G. Amatucci, J.-M. Tarascon, J. Electrochem. Soc. 145 (1998) 472.

[12] H. Maleki, G. Deng, A. Anani, J. Howard, J. Electrochem. Soc. 146 (1999) 3224.

[13] J.R. Dahn, E.W. Fuller, M. Obrovac, U. von Sacken, Solid State Ionics 69 (1994) 265.

[14] Z. Zhang, D. Fouchard, J.R. Rea, J. Power Sources 70 (1998) 16.

[15] H. Maleki, G. Deng, A. Anani, J. Howard, J. Electrochem. Soc. 147 (2000) 4470.

[16] D. Wainwright, J. Power Sources 54 (1995) 192.

[17] W.W.M. Wendladt, Thermal Method of Analysis, vol. 19, John Wiley & Sons, New York, 1974.

[18] Accelerating Rate Calorimetry (ARC) Manual, Arthur D. Little Inc., Cambridge, MA, 1998.

[19] M.N. Richard, J.R. Dahn, J. Power Sources 70 (1999) 135.

[20] D.D. MacNeil, J.R. Dahn, (http://www.Physics.dal.ca/∼dohn/dean/carbon99.html).

[21] Y. Wang, X. Gue, S. Greenbsum, J. Liu, K. Amine, Electrochem. Solid State Lett. 4 (2001) A68.